



Dark Matter Results from 100 Live Days of XENON100 Data

E. Aprile,¹ K. Arisaka,² F. Arneodo,³ A. Askin,⁴ L. Baudis,⁴ A. Behrens,⁴ K. Bokeloh,⁵ E. Brown,⁵ T. Bruch,⁴ G. Bruno,³ J. M. R. Cardoso,⁶ W.-T. Chen,⁷ B. Choi,¹ D. Cline,² E. Duchovni,⁸ S. Fattori,⁹ A. D. Ferella,⁴ F. Gao,¹⁰ K.-L. Giboni,¹ E. Gross,⁸ A. Kish,⁴ C. W. Lam,² J. Lamblin,⁷ R. F. Lang,^{1,*} C. Levy,⁵ K. E. Lim,¹ Q. Lin,¹⁰ S. Lindemann,¹¹ M. Lindner,¹¹ J. A. M. Lopes,⁶ K. Lung,² T. Marrodán Undagoitia,⁴ Y. Mei,^{12,9} A. J. Melgarejo Fernandez,¹ K. Ni,¹⁰ U. Oberlack,^{12,9} S. E. A. Orrigo,⁶ E. Pantic,² R. Persiani,¹³ G. Plante,¹ A. C. C. Ribeiro,⁶ R. Santorelli,⁴ J. M. F. dos Santos,⁶ G. Sartorelli,¹³ M. Schumann,^{4,†} M. Selvi,¹³ P. Shagin,¹² H. Simgen,¹¹ A. Teymourian,² D. Thers,⁷ O. Vitells,⁸ H. Wang,² M. Weber,¹¹ and C. Weinheimer⁵

(The XENON100 Collaboration)

¹Physics Department, Columbia University, New York, New York 10027, USA

²Physics & Astronomy Department, University of California, Los Angeles, California 90095, USA

³INFN, Laboratori Nazionali del Gran Sasso, Assergi, 67100, Italy

⁴Physics Institute, University of Zürich, Winterthurerstr. 190, CH-8057, Switzerland

⁵Institut für Kernphysik, Wilhelms-Universität Münster, 48149 Münster, Germany

⁶Department of Physics, University of Coimbra, R. Larga, 3004-516, Coimbra, Portugal

⁷SUBATECH, Ecole des Mines de Nantes, CNRS/In2p3, Université de Nantes, 44307 Nantes, France

⁸Department of Particle Physics and Astrophysics, Weizmann Institute of Science, 76100 Rehovot, Israel

⁹Institut für Physik, Johannes Gutenberg Universität Mainz, 55099 Mainz, Germany

¹⁰Department of Physics, Shanghai Jiao Tong University, Shanghai, 200240, China

¹¹Max-Planck-Institut für Kernphysik, Saupfercheckweg 1, 69117 Heidelberg, Germany

¹²Department of Physics, Rice University, Houston, Texas 77005-1892, USA

¹³University of Bologna and INFN-Bologna, Bologna, Italy

(Received 14 April 2011; revised manuscript received 18 July 2011; published 19 September 2011)

We present results from the direct search for dark matter with the XENON100 detector, installed underground at the Laboratori Nazionali del Gran Sasso of INFN, Italy. XENON100 is a two-phase time-projection chamber with a 62 kg liquid xenon target. Interaction vertex reconstruction in three dimensions with millimeter precision allows the selection of only the innermost 48 kg as the ultralow background fiducial target. In 100.9 live days of data, acquired between January and June 2010, no evidence for dark matter is found. Three candidate events were observed in the signal region with an expected background of (1.8 ± 0.6) events. This leads to the most stringent limit on dark matter interactions today, excluding spin-independent elastic weakly interacting massive particle (WIMP) nucleon scattering cross sections above $7.0 \times 10^{-45} \text{ cm}^2$ for a WIMP mass of 50 GeV/ c^2 at 90% confidence level.

DOI: 10.1103/PhysRevLett.107.131302

PACS numbers: 95.35.+d, 14.80.Ly, 29.40.-n, 95.55.Vj

Weakly interacting massive particles (WIMPs) are a well-motivated class of particles [1] that could constitute a major fraction of the dark matter in the Universe [2]. These particles can be searched for in underground-based detectors [3] through their coherent scattering off target nuclei. A quasiexponentially falling energy spectrum of nuclear recoils is expected, extending up to a few tens of keV at most for WIMPs scattering off a xenon target [4]. A wide range of WIMP-nucleon cross sections predicted by theoretical models remains untested by current-generation searches, with the most stringent limits on the elastic spin-independent WIMP-nucleon cross section coming from CDMS-II [5], EDELWEISS-II [6], and XENON100 [7].

XENON100 is the current phase of the XENON dark matter program, which aims to improve the sensitivity to

dark matter interactions in liquid xenon (LXe) with two-phase (liquid and gas) time-projection chambers (TPCs) of large mass and low background. A key feature of XENON100 is its ability to localize events with a millimeter resolution in all spatial dimensions, enabling the selection of a fiducial volume in which the radioactive background is minimized. The simultaneous detection of charge and light signals provides discrimination between the expected WIMP-induced nuclear recoil (NR) signal and interactions from the electromagnetic background in the form of electronic recoils (ERs). The first results from XENON100 [7] have shown a sensitivity competitive with that from the full 612 kg days exposure of CDMS-II [5] after only 11.2 live days of data taking. Here, the result of a WIMP search using 100.9 live days of XENON100 data is reported.

XENON100 is filled with 161 kg of ultrapure LXe. Of these, 99 kg are used as an active scintillator veto, surrounding the optically separated 62 kg target in 4π . Thanks to careful material selection [8] and detector design, XENON100 achieves an experimentally verified ER background in the relevant low-energy region of $<5 \times 10^{-3}$ events \times (keV_{ee} kg day)⁻¹ (keV_{ee} = keV electron-equivalent [9]) before signal discrimination [10]. An interaction in the cylindrical LXe target of ~ 30 cm height and ~ 30 cm diameter generates prompt scintillation light (S_1) and ionization electrons, the latter being detected through the process of proportional scintillation (S_2) in the gaseous xenon above the liquid. Both S_1 and S_2 signals are registered by photomultiplier tubes (PMTs) at the bottom of the LXe target for optimal light collection and placed above in the gas phase. The interaction vertex is reconstructed in 3 dimensions, with the (x, y) position determined from the hit pattern of the localized S_2 signal on the top PMT array, and the z coordinate deduced from the drift time between the S_1 and S_2 signals. This allows the fiducialization of the target volume to exploit the excellent self-shielding capabilities of LXe. Because of their different ionization densities, ERs (γ , β background) and NRs (WIMP signal or neutron background) have a different S_2/S_1 ratio, which is used as discrimination parameter.

The 242 PMTs used in XENON100 are 1 in. square Hamamatsu R8520-AL PMTs with a quantum efficiency of $\sim 30\%$ at the Xe light wavelength of 178 nm, and low intrinsic radioactivity [8]. The measured average energy threshold of the LXe veto is ~ 100 keV_{ee}.

The TPC is installed inside a vacuum insulated stainless steel cryostat which is surrounded by a passive shield made of high-purity copper, polyethylene, lead, and water in order to suppress external backgrounds. A constant flow of high-purity nitrogen boil-off gas keeps the ²²²Rn level inside the shield <1 Bq/m³. A 200 W pulse tube refrigerator, installed outside the shield structure, keeps the detector at its operating temperature of -91 °C, with excellent stability over time (fluctuations $<0.05\%$). To bring calibration sources (⁶⁰Co, ¹³⁷Cs, ²⁴¹AmBe) close to the target, a copper tube penetrates the shield and winds around the cryostat. XENON100 is installed underground at the Italian Laboratori Nazionali del Gran Sasso below an average 3600 m water equivalent rock overburden, which reduces the muon flux by a factor $\sim 10^6$.

At low energies, the event trigger is provided by the S_2 signal. The summed signal of 84 central PMTs is shaped and fed into a low-threshold discriminator. The trigger efficiency has been measured to be $>99\%$ at 300 photoelectrons (PE) in S_2 .

Three algorithms are used to reconstruct the (x, y) coordinates of the events. They yield consistent results out to a radius of 14.2 cm, with the active TPC radius being 15.3 cm. The (x, y) resolution was measured with a collimated source and is <3 mm (1σ). The algorithm based on

a neural network gives the most homogeneous response and thus is used for event positioning, while the information from the other algorithms is used for consistency checks. The drift time measurement gives a z -position resolution of 0.3 mm (1σ) and allows for the identification of two interaction vertices if separated by more than 3 mm in z . The positions are corrected for nonuniformities of the drift field, as inferred from a finite-element simulation and validated by data.

XENON100 uses continuous xenon purification through a hot getter. The mean electron lifetime τ_e is indicative of the amount of charge lost to impurities [11]. It increased from 230 μ s to 380 μ s for the data reported here, as measured weekly with ¹³⁷Cs calibrations. A linear fit to the τ_e time evolution yields the z correction for the S_2 signals with negligible systematic uncertainty ($<2.5\%$). (x, y) variations of the S_2 signal are corrected using a map obtained with the 662 keV_{ee} line from ¹³⁷Cs.

The spatial dependence of the S_1 signal due to the nonuniform light collection is corrected for by using a map obtained with the 40 keV_{ee} line from neutrons scattering inelastically on ¹²⁹Xe. It agrees within 3% with maps inferred from data using the 662 keV_{ee} line and the 164 keV_{ee} line, from neutron-activated ^{131m}Xe. The light yield $L_y(122 \text{ keV}_{ee}) = (2.20 \pm 0.09)$ PE/keV_{ee} at the applied drift field of 530 V/cm in the LXe is determined by a fit to the light yields measured with all available calibration lines [7].

The NR energy E_{nr} is inferred from the S_1 signal using $E_{nr} = (S_1/L_y)(1/\mathcal{L}_{eff})(S_{ee}/S_{nr})$. The scintillation efficiency \mathcal{L}_{eff} of NRs relative to that of 122 keV_{ee} γ rays at zero field is taken from the parametrization shown in Fig. 1, which is strongly supported by the most recent measurements by the Columbia group [12] but includes all direct measurements of this quantity [13]. \mathcal{L}_{eff} is logarithmically extrapolated below the lowest measured energy of 3 keV_{nr}, motivated by the trend in the data points as well as studies which simultaneously take into account the light and charge signal [14]. The electric field scintillation

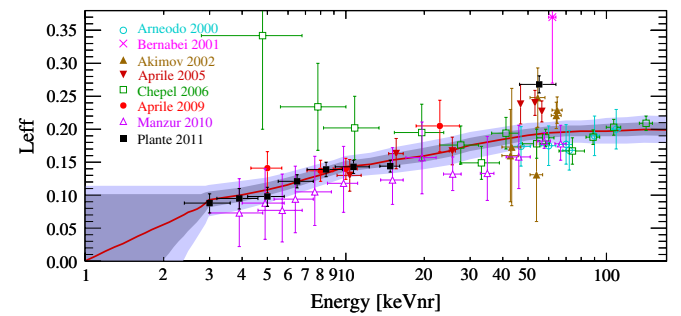


FIG. 1 (color online). All direct measurements of \mathcal{L}_{eff} [12,13] described by a Gaussian distribution to obtain the mean (solid line) and the uncertainty band (1σ and 2σ). Below 3 keV_{nr} the trend is logarithmically extrapolated to $\mathcal{L}_{eff} = 0$ at 1 keV_{nr}.

quenching factors for ERs $S_{ee} = 0.58$ and NRs $S_{nr} = 0.95$ are taken from [15].

The dark matter data presented here were acquired between January 13 and June 8, 2010. About 2% of the exposure was rejected due to variations in detector operation parameters. In addition, 18 live days of data taken in April were rejected due to an increased electronic noise level. With an average data acquisition live time of $\sim 90\%$, and regular calibration runs during the data-taking period, this leads to a dataset of 100.9 live days. This data had been blinded below the 90% ER quantile in $\log_{10}(S2/S1)$ -space for $S1 < 160$ PE.

It was decided *a priori* to derive the dark matter result based on a Profile Likelihood analysis as introduced in [16] but taking into account all relevant backgrounds for this dataset. This analysis does not use a cut based on the $S2/S1$ discrimination. Both, the signal and the background hypothesis would be tested regardless of the observed data. In parallel, an analysis based on the optimum interval method [17] was also performed. The restricted $S2/S1$ space used in the latter analysis, together with the energy interval, defines a benchmark WIMP search region that allows for the direct comparison of the observed signal with the expected background.

From a comparison of the measured background rate with Monte Carlo simulations of the XENON100 electromagnetic background [10], a ^{nat}Kr concentration of (700 ± 100) ppt is inferred for the data reported here, which is higher than reported earlier [7]. The additional Kr was introduced by an air leak during maintenance work on the gas recirculation pump, prior to the start of the data-taking period. This results in an expected ER background of $< 22 \times 10^{-3} \text{ evts} \times (\text{keV}_{ee} \text{ kg day})^{-1}$ before $S2/S1$ discrimination, which is more than an order of magnitude lower than the one of other dark matter search experiments. After the science run presented here, the Kr concentration in the Xe has been reduced by cryogenic distillation to the level reported in [7], as confirmed with a β - γ -coincidence method [18]. XENON100 is taking new data with this reduced background and improved performance.

The imposed requirements to the quality and topology of events are designed to retain the highest possible acceptance of the expected WIMP-induced single-scatter NRs. The majority of cuts were designed and fixed before unblinding the signal region, based on expected signal characteristics, on NR data from a calibration of 2.9 live days with a $^{241}\text{AmBe}$ source, and on low-energy ERs from Compton-scattered gammas from a ^{60}Co source, which were recorded over a total of 5.8 live days spread in time. To reject interactions with a very high energy deposition, the identified $S1$ and $S2$ signals are required to amount to more than half of the total digitized signal. To satisfy the primary requirement of the WIMP signature to be a single-scatter interaction, one $S2$ signal above 300 PE is required, corresponding to about 15 ionization electrons. All other

$S2$ signals have to be small enough to be consistent with PMT afterpulsing or delayed ionization signals from the same single-scatter interaction. The corresponding $S1$ signal must be above 4 PE and must satisfy a twofold PMT coincidence in a ± 20 ns window, without having a coincident signal in the LXe veto. Any other $S1$ -like signal must be consistent with electronic noise or unrelated to the $S2$, based on its $S2/S1$ ratio. In addition, both $S1$ and $S2$ PMT hit patterns as well as the width of the $S2$ pulse are required to be consistent with a single interaction vertex at the reconstructed position. The cumulative cut acceptance, used by both analyses, is shown in Fig. 2 and has an error of $\sim 3\%$. It is estimated based on Monte Carlo simulations, $^{241}\text{AmBe}$ and ^{60}Co calibration data, as well as ERs recorded outside the WIMP search region during the dark matter search. It includes a WIMP mass m_χ dependent $S2$ acceptance which is derived from the expected recoil spectrum and the measured $S2$ vs $S1$ distribution.

The energy window for the WIMP search is chosen between 4–30 PE, corresponding to 8.4–44.6 keV_{nr} based on the \mathcal{L}_{eff} parametrization shown in Fig. 1. The lower bound was assumed to give a sufficient discrimination between genuine $S1$ signals and electronic noise, whereas the upper bound was chosen to include most of the expected WIMP signal. To discriminate ERs from NRs, the parameter $\log_{10}(S2_b/S1)$ is used, with $S2_b$ being the sum of the bottom PMT signals. This choice is motivated by the more uniform signal distribution on these, giving a smaller uncertainty from the (x, y) $S2$ correction. To maximize the sensitivity given the homogeneously distributed ^{85}Kr background, the fiducial volume was optimized on ER background data and set to 48 kg, and the ER rejection level was set to 99.75%. The acceptance to NRs below this line is calculated based on single-scatter NRs from $^{241}\text{AmBe}$ data and is also shown in Fig. 2. The profile likelihood approach tests the full $S2/S1$ space and does not employ this cut.

The expected background in the WIMP search region is the sum of Gaussian leakage from the ER background, of non-Gaussian leakage and of NRs from neutron

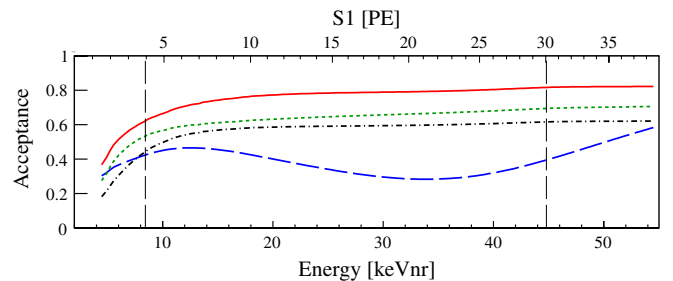


FIG. 2 (color online). Acceptance of all data quality cuts used for the analysis for $m_\chi \geq 50 \text{ GeV}/c^2$ (solid red line), $m_\chi = 10 \text{ GeV}/c^2$ (dotted green line), $m_\chi = 7 \text{ GeV}/c^2$ (dash-dotted black line). The optimum interval analysis additionally uses a $S2/S1$ ER discrimination cut. Its NR acceptance is also shown (dashed blue line).

interactions. The latter, estimated by Monte Carlo simulations, takes into account neutron spectra and total production rates from (α, n) and spontaneous fission reactions in the detector and shield materials, and is based on the measured radioactivity concentrations [8]. The impact of muon-induced neutrons is obtained from simulations and contributes 70% to the total. Taking into account the measured trigger efficiency and the energy threshold in the active LXe veto, the overall prediction is $(0.31^{+0.22}_{-0.11})$ single-scatter NRs in the 100.9 days data sample before a $S2/S1$ -cut in the energy region of interest and 48 kg fiducial mass, of which $(0.11^{+0.08}_{-0.04})$ are expected in the benchmark WIMP search region.

The normalized ER band, obtained by subtracting its mean as inferred from ^{60}Co calibration data, is well described by a Gaussian distribution in $\log_{10}(S2_b/S1)$ space. Gaussian leakage, dominated by the ^{85}Kr background, is predicted from the number of background events outside the blinded WIMP search region, taking into account the blinding cut efficiency and the ER rejection level. It is (1.14 ± 0.48) events in the benchmark WIMP search region, where the error is dominated by the statistical uncertainty in the definition of the discrimination line. Non-Gaussian (anomalous) leakage can be due to double-scatter gamma events with one interaction in a charge insensitive region, e.g., below the cathode, and one in the active target volume. Such events have a lower effective $S2/S1$ ratio, since only one interaction contributes to the $S2$, but both to the $S1$. Their contribution has been estimated using ^{60}Co calibration data, and accounting for the fact that the background of this data set is dominated by ^{85}Kr which undergoes β decay and does not contribute to such event topologies. The spatial distribution of leakage events for background and calibration data is similar within 10%. This is verified by Monte Carlo simulations and by data, selecting potential leakage candidates by their $S1$ PMT hit pattern. Anomalous leakage is estimated to give $(0.56^{+0.21}_{-0.27})$ events, where the uncertainty takes into account the difference in the background and calibration distributions, and that the leakage might be overestimated because of the uncertainty in the ^{85}Kr concentration. In summary, the total background prediction in the WIMP search region for 99.75% ER rejection, 100.9 days of exposure, and 48 kg fiducial mass is (1.8 ± 0.6) events. This expectation was verified by unblinding the high energy sideband from 30–130 PE before unblinding the WIMP search region. The profile likelihood analysis employs the same data and background assumptions to obtain the prediction for the Gaussian, non-Gaussian, and neutron background for every point in the $\log_{10}(S2_b/S1)$ parameter space.

After unblinding the predefined WIMP search region, a population of events was observed that passed the $S1$ coincidence requirement only because of correlated electronic noise that is picked up from an external 100 kHz source, as verified by an inspection of the

digitized PMT signals. These events are mostly found below the $S1$ analysis threshold, with 3 events from this population leaking into the WIMP search region close to the 4 PE lower bound. This population can be identified and rejected with a cut on the $S1$ PMT coincidence level, that takes into account correlated pickup noise, and by cutting on the width of the $S1$ candidate. These post-unblinding cuts have a combined acceptance of 99.75% for NRs while removing the entire population of noise events.

With these additional cuts, 3 events pass all quality criteria for single-scatter NRs and fall in the WIMP search region; see Fig. 3. This observation remains unchanged for moderate variations in the definition of any of the data quality cuts. These events were observed on January 23, February 12, and June 3, at $30.2 \text{ keV}_{\text{nr}}$, $34.6 \text{ keV}_{\text{nr}}$, and $12.1 \text{ keV}_{\text{nr}}$, respectively. The event distribution in the TPC is shown in Fig. 4. Given the background expectation of (1.8 ± 0.6) events, the observation of 3 events does not constitute evidence for dark matter, as the chance probability of the corresponding Poisson process to result in 3 or more events is 28%.

The statistical analysis using the profile likelihood method [16] does not yield a significant signal excess either, the p value of the background-only hypothesis is 31%. A limit on the spin-independent WIMP-nucleon elastic scattering cross section σ is calculated where

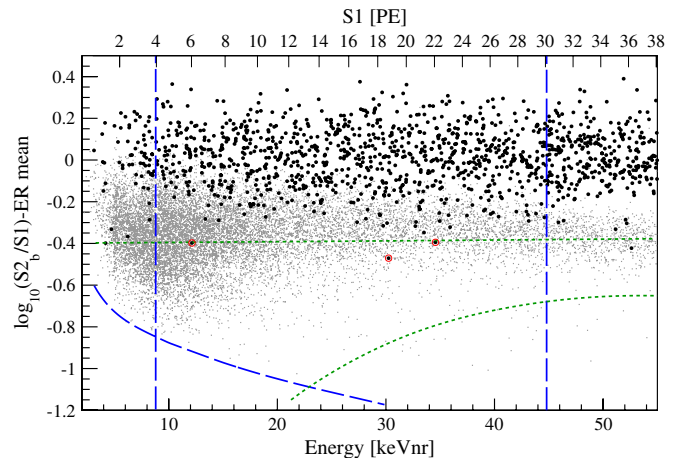


FIG. 3 (color online). Observed event distribution using the discrimination parameter $\log_{10}(S2_b/S1)$, flattened by subtracting the ER band mean, as a function of NR equivalent energy (keV_{nr}). All quality cuts, including those defined after unblinding, are used. Gray points indicate the NR distribution as measured with a $^{241}\text{AmBe}$ neutron source. The WIMP search region is defined by the energy window 8.4–44.6 keV_{nr} (4–30 PE) and the lower bound of the software threshold $S2 > 300$ PE (blue dashed line). The optimum interval analysis additionally uses the 99.75% rejection line from above and the 3σ contour of the NR distribution from below (green dotted line). Three events fall into this WIMP search region (red circles), with (1.8 ± 0.6) events expected from the background.

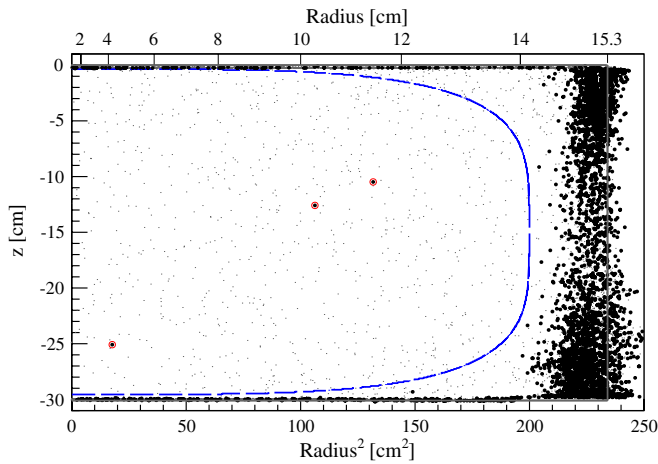


FIG. 4 (color online). Distribution of all events (gray dots) and events below the 99.75% rejection line (black dots) in the TPC observed in the 8.4–44.6 keV_{nr} energy range during 100.9 live days. All cuts are used here, including the ones introduced post-unblinding to remove a population due to electronic noise. The 48 kg fiducial volume (blue dashed line) and the TPC dimensions (gray line) are also indicated.

WIMPs are assumed to be distributed in an isothermal halo with $v_0 = 220$ km/s, Galactic escape velocity $v_{\text{esc}} = (544^{+64}_{-46})$ km/s, and a density of $\rho_\chi = 0.3$ GeV/cm³. The S1 energy resolution, governed by Poisson fluctuations of the PE generation in the PMTs, is taken into account.

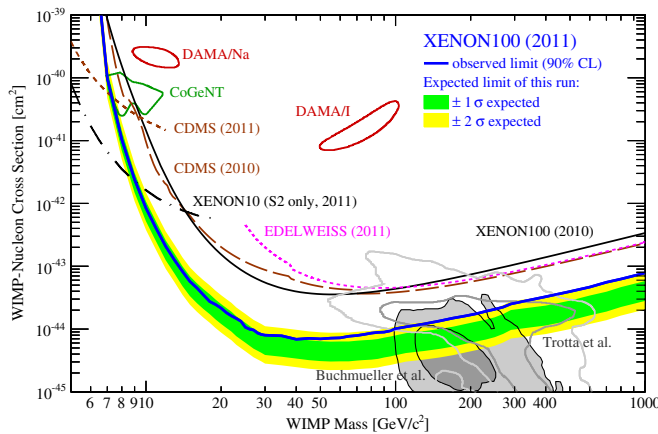


FIG. 5 (color online). Spin-independent elastic WIMP-nucleon cross section σ as a function of WIMP mass m_χ . The new XENON100 limit at 90% C.L., as derived with the profile likelihood method taking into account all relevant systematic uncertainties, is shown as the thick (blue) line together with the expected sensitivity of this run (green-yellow band). The limits from XENON100 (2010) [7], EDELWEISS (2011) [6], CDMS (2009) [5] (recalculated with $v_{\text{esc}} = 544$ km/s, $v_0 = 220$ km/s), CDMS (2011) [22], and XENON10 (2011) [23] are also shown. Expectations from CMSSM are indicated at 68% and 95% C.L. (shaded gray [19], gray contour [24]), as well as the 90% C.L. areas favored by CoGeNT [21] and DAMA (no channeling) [20].

Uncertainties in the energy scale as indicated in Fig. 1, in the background expectation, and in v_{esc} are profiled out and incorporated into the limit. The resulting 90% confidence level (C.L.) limit is shown in Fig. 5 and has a minimum $\sigma = 7.0 \times 10^{-45}$ cm² at a WIMP mass of $m_\chi = 50$ GeV/ c^2 . The impact of \mathcal{L}_{eff} data below 3 keV_{nr} is negligible at $m_\chi = 10$ GeV/ c^2 . The sensitivity is the expected limit in absence of a signal above background and is also shown in Fig. 5. Because of the presence of two events around 30 keV_{nr}, the limit at higher m_χ is weaker than expected. Within the systematic differences of the methods, this limit is consistent with the one from the optimum interval analysis, which calculates the limit based only on events in the WIMP search region. Its acceptance-corrected exposure, weighted with the spectrum of a $m_\chi = 100$ GeV/ c^2 WIMP, is 1471 kg days. This result excludes a large fraction of previously unexplored WIMP parameter space, and cuts into the region where supersymmetric WIMP dark matter is accessible by the LHC [19]. Moreover, the new result challenges the interpretation of the DAMA [20] and CoGeNT [21] results as being due to light mass WIMPs.

We gratefully acknowledge support from NSF, DOE, SNF, Volkswagen Foundation, FCT, Région des Pays de la Loire, STCSM, DFG, and the Weizmann Institute of Science. We are grateful to the Laboratori Nazionali del Gran Sasso for hosting and supporting XENON.

*rafael.lang@astro.columbia.edu

†marc.schumann@physik.uzh.ch

- [1] G. Steigman and M. S. Turner, *Nucl. Phys.* **B253**, 375 (1985); G. Jungman, M. Kamionkowski, and K. Griest, *Phys. Rep.* **267**, 195 (1996).
- [2] N. Jarosik *et al.*, *Astrophys. J. Suppl. Ser.* **192**, 14 (2011); K. Nakamura *et al.* (Particle Data Group), *J. Phys. G* **37**, 075021 (2010).
- [3] M. W. Goodman and E. Witten, *Phys. Rev. D* **31**, 3059 (1985).
- [4] J. D. Lewin and P. F. Smith, *Astropart. Phys.* **6**, 87 (1996).
- [5] Z. Ahmed *et al.* (CDMS Collaboration), *Science* **327**, 1619 (2010).
- [6] E. Armengaud *et al.* (EDELWEISS Collaboration) *Phys. Lett. B* **702**, 329 (2011).
- [7] E. Aprile *et al.* (XENON100 Collaboration), *Phys. Rev. Lett.* **105**, 131302 (2010).
- [8] E. Aprile *et al.* (XENON100 Collaboration), *Astropart. Phys.* **35**, 43 (2011).
- [9] E. Aprile *et al.*, *Phys. Rev. C* **79**, 045807 (2009).
- [10] E. Aprile *et al.* (XENON100 Collaboration), *Phys. Rev. D* **83**, 082001 (2011).
- [11] E. Aprile and T. Doke, *Rev. Mod. Phys.* **82**, 2053 (2010).
- [12] G. Plante *et al.*, arXiv:1104.2587.
- [13] F. Arneodo *et al.*, *Nucl. Instrum. Methods Phys. Res., Sect. A* **449**, 147 (2000); D. Akimov *et al.*, *Phys. Lett. B* **524**, 245 (2002); R. Bernabei *et al.*, *Eur. Phys. J. direct C*

- 3, 11 (2001); E. Aprile *et al.*, *Phys. Rev. D* **72**, 072006 (2005); V. Chepel *et al.*, *Astropart. Phys.* **26**, 58 (2006);
A. Manzur *et al.*, *Phys. Rev. C* **81**, 025808 (2010).
- [14] F. Bezrukov *et al.*, *Astropart. Phys.* **35**, 119 (2011).
[15] E. Aprile *et al.*, *Phys. Rev. Lett.* **97**, 081302 (2006).
[16] E. Aprile *et al.* (XENON100 Collaboration), *Phys. Rev. D* **84**, 052003 (2011).
[17] S. Yellin, *Phys. Rev. D* **66**, 032005 (2002).
[18] G. Alimonti *et al.*, *Astropart. Phys.* **16**, 205 (2002).
- [19] O. Buchmueller *et al.*, Report No CERN-PH-TH/2010-321, KCL-PH-TH/2011-04, [arXiv:1102.4585](https://arxiv.org/abs/1102.4585).
[20] C. Savage *et al.*, *J. Cosmol. Astropart. Phys.* **04** (2009) 010.
[21] C.E. Aalseth *et al.* (CoGeNT Collaboration), *Phys. Rev. Lett.* **106**, 131301 (2011).
[22] Z. Ahmed *et al.* (CDMS Collaboration), *Phys. Rev. Lett.* **106**, 131302 (2011).
[23] J. Angle *et al.* (XENON10 Collaboration), *Phys. Rev. Lett.* **107**, 051301 (2011).
[24] R. Trotta *et al.*, *J. High Energy Phys.* **12** (2008) 024.